

## Geodetic observations of an earthquake cycle at the Sumatra subduction zone: Role of interseismic strain segmentation

Linette Prawirodirdjo,<sup>1</sup> Robert McCaffrey,<sup>2</sup> C. David Chadwell,<sup>3</sup> Yehuda Bock,<sup>1</sup> and Cecep Subarya<sup>4</sup>

Received 5 October 2008; revised 27 June 2009; accepted 22 October 2009; published 19 March 2010.

[1] We use survey mode and continuous GPS data from 1991 to 2007 to examine fault segmentation in the earthquake cycle at the Sumatra megathrust, site of the 26 December 2004  $M_w$  9.1 Sumatra-Andaman, the 28 March 2005  $M_w$  8.7 Nias-Simeulue, and the 12 September 2007  $M_w$  8.4 Mentawai earthquakes. These data, including new observations from 2006 and 2007, allow us to observe the final few years of one earthquake cycle and the beginning of the next. Our analysis reveals that the megathrust is segmented, a characteristic that may persist through multiple earthquake cycles. The Nias-Simeulue earthquake ruptured approximately the same region that broke in 1861, a 300 km long segment abutting the Sumatra-Andaman rupture zone. Farther southeast, the Mentawai segment of the megathrust (0.5°S–5°S), which produced  $M > 8$  earthquakes in 1797 and 1833, is fully locked in the interseismic period but is flanked by two freely slipping regions, the Batu Islands in the NW and Enggano in the SE. The 12 September 2007 Mentawai earthquake sequence ruptured only the southern one third of the 1833 rupture zone. We model postseismic deformation from the Sumatra-Andaman and Nias-Simeulue earthquakes and find that afterslip was concentrated updip and downdip, respectively, from the main shocks. Comparing the velocity fields before and after 2001, we find the subduction zone underneath the Batu Islands and Enggano, which, prior to the earthquakes, was partially to fully coupled, appears now to be slipping freely. Thus, while the segmentation of the subduction zone is preserved, interseismic coupling on the subduction fault may vary with time.

**Citation:** Prawirodirdjo, L., R. McCaffrey, C. D. Chadwell, Y. Bock, and C. Subarya (2010), Geodetic observations of an earthquake cycle at the Sumatra subduction zone: Role of interseismic strain segmentation, *J. Geophys. Res.*, 115, B03414, doi:10.1029/2008JB006139.

### 1. Introduction

[2] The great  $M_w$  9.22 Sumatra-Andaman earthquake of 26 December 2004 [Ammon *et al.*, 2005; Stein and Okal, 2005; Banerjee *et al.*, 2005; Subarya *et al.*, 2006; Chlieh *et al.*, 2007] and the  $M_w$  8.7 Nias-Simeulue earthquake of 28 March 2005 [Briggs *et al.*, 2006] ruptured adjacent segments of the Sumatra subduction zone (Figure 1). Our previous geodetic studies of interseismic deformation in the region indicated that the pattern of strain accumulation on the Sumatra subduction zone between 0.5°S and 2°N was significantly different from that south of 0.5°S [Prawirodirdjo

*et al.*, 1997; Bock *et al.*, 2003]. This apparent spatial variation in the interseismic velocity field coincided with the area between the rupture zones of previous great earthquakes that occurred on the Sumatra subduction zone in 1833 and 1861 (Figures 1 and 2a) [Newcomb and McCann, 1987]. The rupture boundary appeared as an abrupt change in the trench-normal strain accumulation rate (as inferred from the trench-normal GPS velocities) well into the interseismic cycle, suggesting that segmentation of earthquake slip distribution may persist through multiple earthquake cycles. The Nias earthquake occurred in approximately the same region that broke in 1861, a 300 km long segment directly SE of and abutting the Sumatra-Andaman rupture zone [Subarya *et al.*, 2006]. The Mentawai segment of the megathrust (0.5°S–5°S) that produced  $M > 8$  earthquakes in 1797 and 1833 remained fully locked and flanked by two regions of low coupling, the Batu Islands in the NW and Enggano Island in the SE. The 12 September 2007 Mentawai earthquake sequence only partially ruptured the 1833 rupture zone [Konca *et al.*, 2008; Sieh *et al.*, 2008].

[3] In this work we further investigate the role of interseismic strain segmentation on the Sumatra megathrust in

<sup>1</sup>Cecil H. and Ida M. Green Institute of Geophysics and Planetary Physics, Scripps Institution of Oceanography, La Jolla, California, USA.

<sup>2</sup>Department of Earth and Environmental Sciences, Rensselaer Polytechnic Institute, Troy, New York, USA.

<sup>3</sup>Marine Physical Laboratory, Scripps Institution of Oceanography, La Jolla, California, USA.

<sup>4</sup>National Coordinating Agency for Surveys and Mapping, Cibinong, Indonesia.

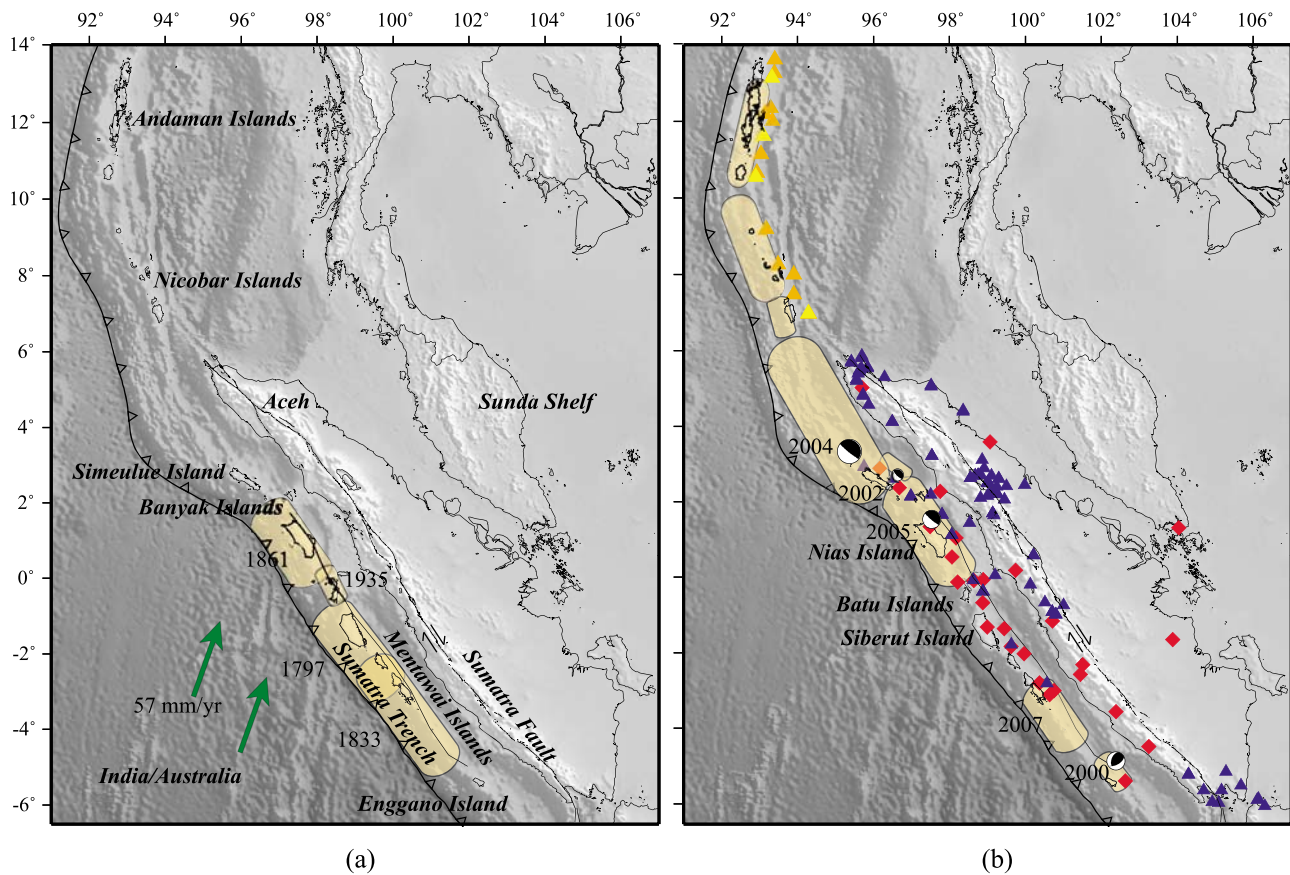


**Figure 1.** Rupture zones (yellow regions) of major (a) historical and (b) recent interplate earthquakes along the Sumatra subduction zone with GPS monuments surveyed by our group (blue triangles), *Gahalaut et al.* [2006] (orange triangles), *Jade et al.* [2005] (yellow triangles), and SuGAr CGPS stations (red diamonds). Trench-parallel solid line landward of the Mentawai islands is the Mentawai fault. Green arrows show motion of the India/Australia plate relative to the Sunda Shelf.

light of the sequence of large earthquakes in 2004–2007. We model the interseismic velocity field for the Sumatra megathrust prior to and after the Sumatra-Andaman earthquake using survey mode and continuous GPS data from the period 1991–2007 processed in the ITRF2005 reference frame. These data include yet unpublished survey mode GPS data gathered by the Indonesian National Coordinating Agency for Surveys and Mapping (BAKOSURTANAL) throughout Sumatra from March–April 2006 and April–May 2007, approximately 1 and 2 years after the Nias earthquake. We also reestimate the coseismic and postseismic slip distribution of the Nias earthquake using these new survey mode data, supplemented by continuous GPS (CGPS) data from the Sumatra GPS array (SuGAr, <http://www.tectonics.caltech.edu/sumatra/sugar.html>) operated by the California Institute of Technology's (Caltech) Tectonics Observatory (TO). These 2006 and 2007 survey GPS data have not been previously presented in the many published geodetic studies of the Sumatra-Andaman and Nias earthquakes. Compared to the CGPS data, these survey GPS data comprise more stations on the fore-arc islands and on the main island of Sumatra, thus providing better spatial coverage of the near-field deformation from the Nias earthquake. Furthermore, surveys in the northern (Aceh) region in 2006 and 2007 provide a view of the postseismic deformation from the

2004 Aceh earthquake. This study therefore supplements the analysis performed by *Briggs et al.* [2006], who examined the coseismic deformation due to the Nias earthquake recorded by coral microatolls and CGPS; *Hsu et al.* [2006], who studied afterslip following the Nias earthquake recorded by CGPS; and *Konca et al.* [2007a], who studied the Nias rupture kinematics using seismic and geodetic data. Our new data also allow us to observe the transition from the immediate postseismic period (characterized by aseismic unloading of the fault) into the interseismic period where loading of the fault picks up again. Finally, we perform a kinematic analysis of the 120 s rate CGPS data to examine any possible motion that took place in the few hours immediately before and after the Nias earthquake.

## 2. Data

### **2.1. Survey Mode GPS**

[4] Convergence between the Australian-Indian plate and the Sunda Shelf along the Java Trench is nearly orthogonal to the plate boundary at a rate of about 63 mm/yr [Bock *et al.*, 2003; Socquet *et al.*, 2006]. To the northwest along the island of Sumatra, the direction of convergence becomes increasingly oblique to the trench and the relative plate motion is partitioned [Fitch, 1972; McCaffrey, 1992] into

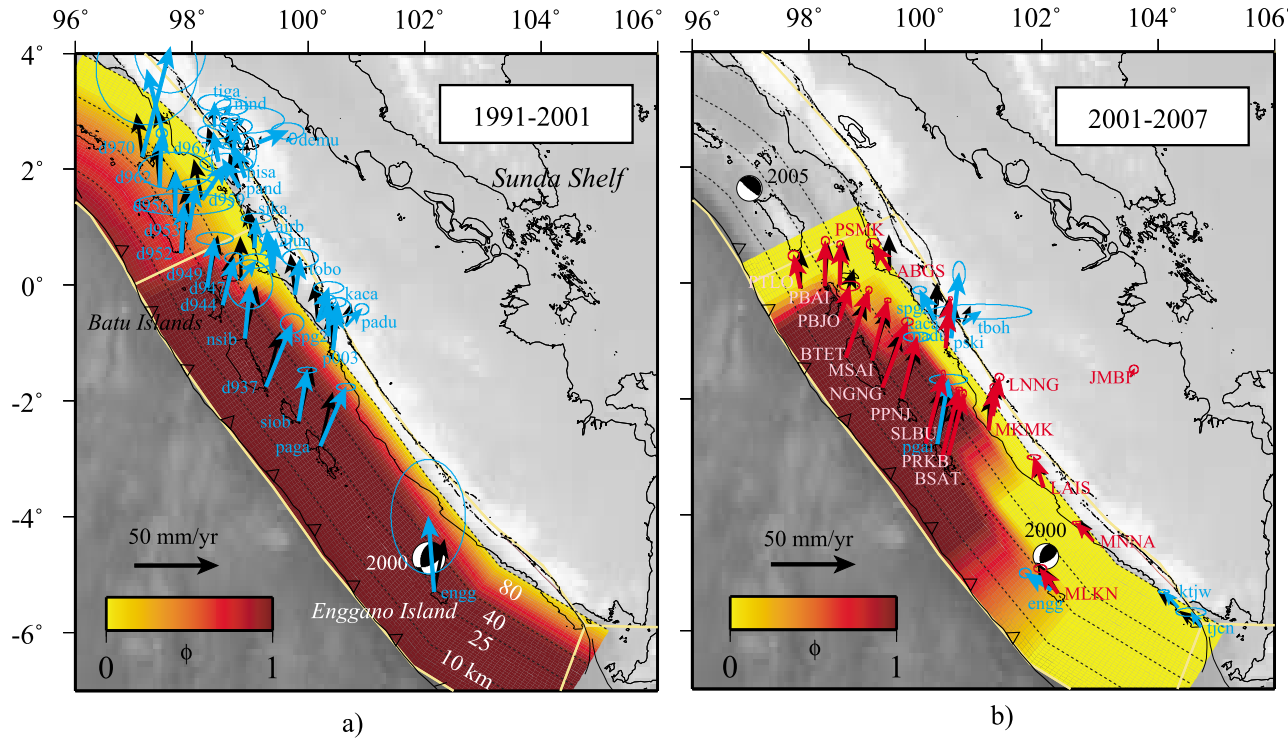


**Figure 2.** Interseismic velocity field relative to Sunda Shelf. Yellow line delineates the fore-arc block defined by the model. Shading on the fore arc represents the value of the coupling coefficient  $\varphi$  used in the model. The rotation pole for the Sunda Shelf was estimated from the velocities at BAKO, NTUS, SAMP, and JMBI. Focal mechanisms are given for large earthquakes that occurred in 2000–2006. (a) Blue vectors are velocity vectors from survey GPS stations spanning the period 1991–2001. Black vectors are predicted velocity vectors calculated by model. Dashed lines indicate slab contours, with depths (km) labeled at lower right. (b) Red vectors show velocity field from SuGAr stations from ~2002 to 2007; blue vectors show velocity field from survey GPS stations from ~2001 to 2007 (see Table S1 in the auxiliary material for time spans represented by velocities); black vectors show velocity vectors predicted by the interseismic model.

nearly perpendicular thrusting on the subduction zone at 45 mm/yr [Bock *et al.*, 2003] and trench-parallel, right-lateral slip along the Sumatran fault (SF) at 11–28 mm/yr [Sieh and Natawidjaja, 2000; Genrich *et al.*, 2000]. GPS geodetic surveys performed in 1989–2001 by our group, which includes BAKOSURTANAL, Scripps Institution of Oceanography (SIO), and Rensselaer Polytechnic Institute (RPI), to study oblique subduction and associated seismic hazards in Sumatra and the islands on the Sumatra fore arc provide a record of interseismic deformation directly above the subduction zone (Figure 2a) [Praviriodirdjo *et al.*, 1997; Genrich *et al.*, 2000; Bock *et al.*, 2003]. Following the Sumatra-Andaman earthquake, several of these GPS monuments were resurveyed between 28 January and 19 February 2005 [Subarya *et al.*, 2006]. After the Nias earthquake of 28 March 2005, the GPS monuments (many of which were located directly above the Nias-Simeulue rupture zone) were surveyed again from 16 April to 4 May 2005, providing displacements for that event also. Most recently, GPS monuments in all of Sumatra were surveyed again from 6 March to 19 April 2006 and from 14 April to 20 May 2007. The occupation schedule for the GPS survey stations on Sumatra and the Mentawai islands from 1991 to

2007 is summarized in Table S1 in the auxiliary material.<sup>1</sup> Earlier occupations in 1989 and 1990 are not used because of the combined effects of poor satellite coverage, sparse global data, and GPS selective availability (SA).

[5] We process the raw GPS data with the suite of programs GAMIT version 10.32 and GLOBK/GLORG version 5.12 (<http://www-gpsg.mit.edu/~simon/gtk/index.htm>) in 24 h segments, along with data from 10 additional CGPS sites in Java, Cocos Island, Diego Garcia, Singapore, India, Australia, and Guam. These solutions are then combined with global GPS network solutions produced routinely at the Scripps Orbit and Permanent Array Center (SOPAC, <http://sopac.ucsd.edu>) to determine station position time series with respect to the ITRF2005 reference frame [Altamimi *et al.*, 2007]. Previously analyzed GPS survey data as far back as 1991 were also reprocessed with the latest versions of GAMIT and GLOBK, and station positions were estimated in ITRF2005 to be consistent with the processing of more recent data. The data reanalysis also included some major modeling changes compared to previous studies,

<sup>1</sup>Auxiliary materials are available in the HTML. doi:10.1029/2008JB006139.

including the adoption of absolute phase center antenna models [Schmid *et al.*, 2007], latest Differential Code Biases (DCB) tables ([http://cmslive2.unibe.ch/unibe/phlnat/aiub/content/e15/e59/e440/e447/e573/index\\_eng.html](http://cmslive2.unibe.ch/unibe/phlnat/aiub/content/e15/e59/e440/e447/e573/index_eng.html)), GMF global troposphere mapping function [Boehm *et al.*, 2006], and a new ocean tide loading model, FES2004, with center of mass correction [Scherneck *et al.*, 2000].

## 2.2. Continuous GPS

[6] The survey mode GPS data are supplemented by continuous GPS (CGPS) data from the Sumatra GPS array established by Caltech's TO in 2002 (Figure 1). The SuGAr data are crucial to the study of interseismic motion and this great earthquake sequence, providing a check for the temporally sparse survey mode data. Initially, SuGAr was concentrated south of the Batu Islands where there were no significant displacements due to the Sumatra-Andaman earthquake. Immediately after the 2004 Sumatra-Andaman earthquake, TO added four new CGPS stations in the North (in Nias, Simeulue, and Aceh) which later recorded large coseismic and postseismic displacements from the March 2005 Nias earthquake. One publicly available CGPS station in northern Sumatra, SAMP, operated by BAKOSURTANAL since 2002, also recorded coseismic offsets and postseismic motions from both earthquakes.

[7] The raw CGPS data are processed using the GAMIT/GLOBK software as described in section 2.1 for the survey mode GPS data, and the daily position time series are used to estimate interseismic rates and coseismic and postseismic deformation using the methods described by Nikolaidis [2002].

## 3. Geodetic Analysis

### 3.1. Interseismic Analysis

[8] The last GPS surveys in Sumatra before the giant earthquake sequence of 2004 and 2005 were performed in 2001; thus, we compare the survey GPS-derived velocities before and after that date. It must be noted, though, that not all stations were occupied during each survey (Table S1). We plot all velocities relative to a stationary Sunda Shelf plate. Between 1991 and 2001, the GPS-measured velocity field showed different patterns of deformation on the northern and southern parts of the fore arc (Figure 2a). The velocities on the southern fore arc (between 0.5°S and 6°S) were consistent with a fully locked subduction thrust fault, while vectors on the northern fore arc were rotated anticlockwise relative to those in the south [see also Prawirodirdjo *et al.*, 1997; Bock *et al.*, 2003] and were more consistent with only partial (about 50%) coupling on the subduction fault.

[9] Figure 2b shows velocities for 2001–2007 from survey mode GPS data supplemented by velocities from the SuGAr CGPS stations from approximately 2002–2007 (velocities for the Batu Islands are estimated using data from 2002 to March 2005, just before the Nias earthquake). The velocity field along the southern part of the fore arc between 0° and 3.5°S is similar for both time periods (Figure 2a). At the Batu Islands the velocity field shows some temporal variation. In the 1991–2001 velocity field, vectors on the Batu Islands pointed NNE (Figure 2a) while in the later velocity field (including velocities derived from CGPS sta-

tions) they point more nearly northward (Figure 2b) and are markedly slower than those to the south. The current, well constrained observations from the CGPS array confirms that the interseismic deformation along the Sumatra fore arc is segmented and one clear segmentation boundary occurs in the vicinity of the Batu Islands.

[10] The 2001–2007 velocity on Enggano Island is also different from what it was in the 1990s. The more recent velocity (Figure 2b) points nearly NW, similar to velocities of sites on coastal Sumatra, but significantly different from the velocities on Siberut and the Pagai Islands. This temporal change in the velocity may be related to the large ( $M_w = 7.9$ ) earthquake that occurred in this region on 4 June 2000. This is discussed further in sections 4.1 and 5.

### 3.2. Coseismic Analysis

[11] The GPS surveys following the Sumatra-Andaman earthquake were concentrated in Aceh, on the mainland, but included three stations located on the fore arc: r171, d972 and d962 (Figure 3). Some stations, such as the “r” stations (those starting with the letter r), lhok, and lang, were surveyed only once in the 1990s for mapping control. To estimate displacements due to the Sumatra-Andaman and Nias earthquakes at these stations, we use the interseismic model discussed in section 4.1 to extrapolate station positions to the time just prior to the 2004–2005 earthquake sequence.

[12] Since the postearthquake surveys were performed several days after the main shock, the displacements recorded at the survey GPS stations presumably contain the coseismic displacements plus several days of postseismic deformation. The displacements in Aceh following the 2004 earthquake were about 4 m, and the largest measured displacement, at r171, was 5.7 m (Figure 3). In contrast, displacements at d972 and d962 during the Sumatra-Andaman earthquake were only 28 cm and 5 cm, respectively, suggesting that the rupture zone ended abruptly in the region of Simeulue Island (Figure 3) [Subarya *et al.*, 2006]. Station r171 also uplifted about 2 m, while the other survey stations subsided at the centimeter level during the Sumatra-Andaman earthquake. After the March 2005 Nias earthquake, 32 GPS monuments on Sumatra and the fore-arc islands were reoccupied within 20–30 days following the earthquake (Figure 3). Ten of these stations were not resurveyed during the period between the Sumatra and Nias earthquakes; thus, their recorded displacements potentially include the effects of both earthquakes. However, all but one of these stations, tptn, are located well south of the Sumatra-Andaman earthquake displacement field shown by Subarya *et al.* [2006], so we assume that displacements at these stations are largely due to the Nias earthquake.

[13] The largest displacements due to the Nias earthquake were recorded on the islands of Nias (survey station nmet and CGPS station LHWA) and SarangBaung (survey station d962, 20 km NE of Nias). The horizontal displacements at nmet, d962 and LHWA reached 4.0 to 4.5 m. Station LHWA was also uplifted by about 3 m. CGPS station BSIM on southern Simeulue reveals 2.3 m of horizontal displacement and 1.6 m of uplift (inset, Figure 3).

[14] The recorded displacements (coseismic plus several days of postseismic) following the Nias earthquake decreased steeply to the NW and SE of the main rupture zone. At the

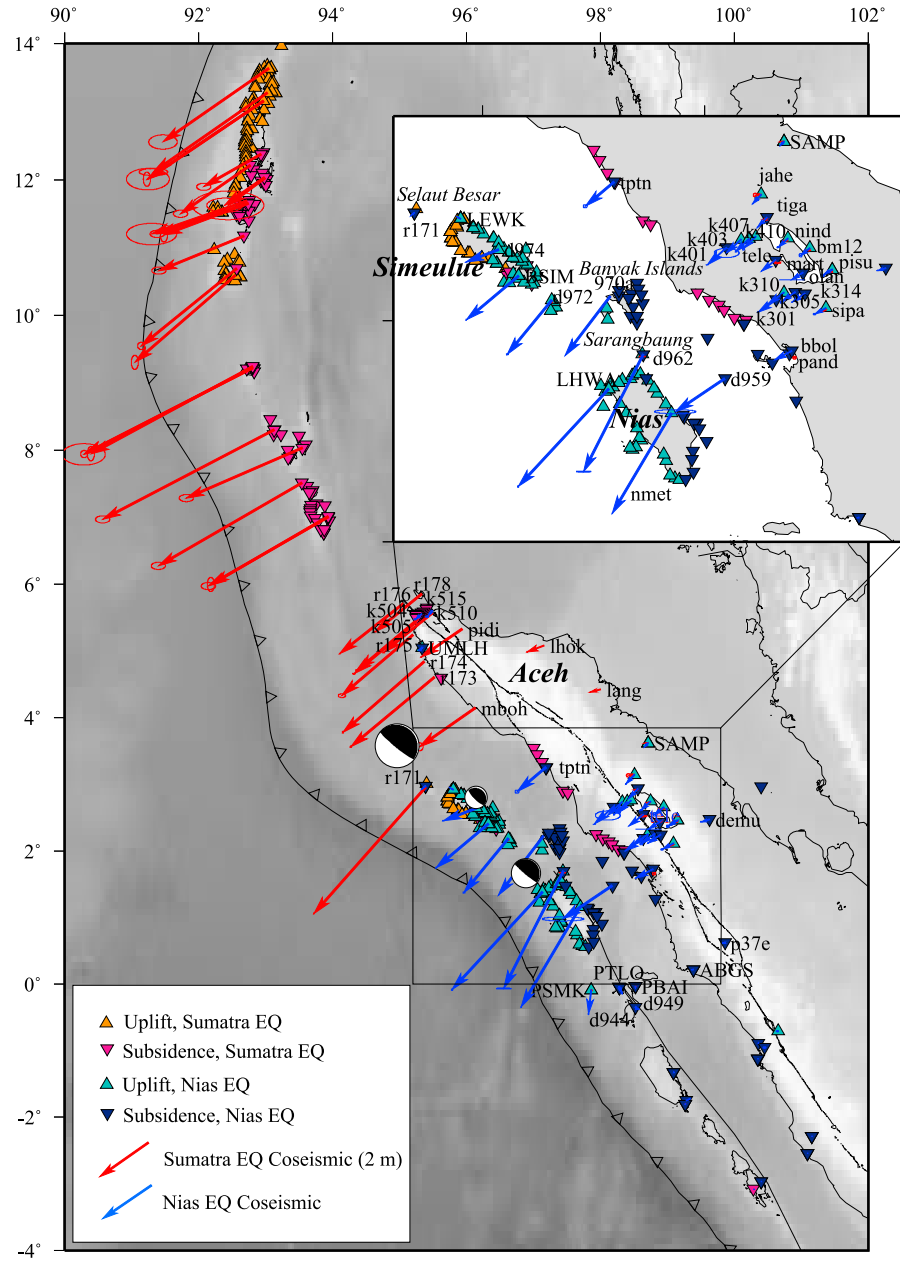


**Figure 3.** Coseismic horizontal and vertical displacements from Sumatra and Nias earthquakes. Inset shows close-up of area outlined in rectangle. Continuous GPS stations are labeled with all capital letters, survey GPS stations are labeled in lower case. Survey stations north of 6°N are from *Gahalaut et al.* [2006] and *Jade et al.* [2005]. Uplift and subsidence are indicated by triangles as well from coral observations by *Meltzner et al.* [2006] and *Meltzner et al.* [2007].

northern end of the displacement field, station r171 on the island Selaut Besar, which moved more than 5 m during the Sumatra-Andaman earthquake [*Subarya et al.*, 2006], was displaced <20 mm during the Nias-Simeulue earthquake. In the SE, displacements at the CGPS stations on the Batu islands were <25 cm, suggesting that the rupture zone terminated abruptly just north of the Batu Islands. Uplift is observed at stations d974, d972, and nmet, and subsidence is observed at all other survey stations on the fore arc (Table S3 in the auxiliary material). Combined with the vertical deformation measured at the CGPS stations, these observations place the pivot line (transition between subsidence and uplift)

just NE of the islands of Nias and Simeulue. The station r171, just NW of Simeulue, subsided during the earthquake, suggesting that the edge of the rupture zone is located SE of it.

[15] A striking feature of Figure 3 is the narrow boundary between the displacement fields of the two great earthquakes. The rupture boundary falls north of Simeulue Island, near station r171, and on Sumatra the boundary is located between stations tptn and mboh. *Newcomb and McCann* [1987] estimated the northern end of the 1861 earthquake to be near the Banyak Islands. The Nias earthquake therefore, while similar to the 1861 earthquake, ruptured a slightly larger region (Figure 1). Also notable is that

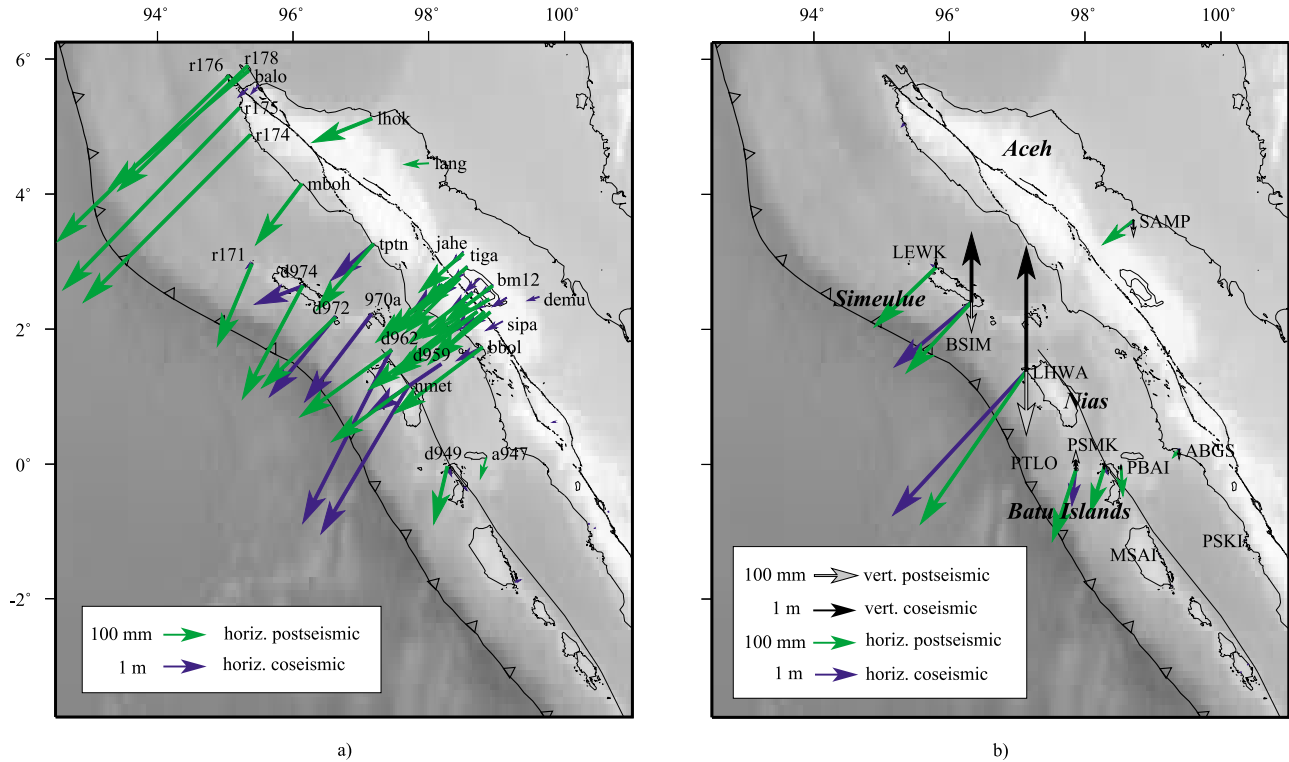


**Figure 4.** (a) Horizontal coseismic and postseismic displacements measured at survey GPS stations during 1 year period following Nias earthquake. (b) Horizontal and vertical coseismic displacements at SuGAr continuous stations during Nias earthquake, and postseismic horizontal and vertical displacements accumulated in the 1 year period following the Nias earthquake.

the southern terminus of the Nias earthquake, just north of the Batu islands, coincides with the region where the change in interseismic velocity vector azimuths is seen in Figure 2b. The rupture zones of the 2004 and 2005 earthquakes appear to be related to rupture zones of past earthquakes, as well as to the deformation pattern observed during the interseismic phase of the earthquake cycle.

### 3.3. Postseismic Analysis

[16] Survey mode GPS stations in Sumatra were resurveyed in March–April 2006, enabling us to measure the displacement that occurred during the 1 year following the Nias earthquake (Figure 4a). Between April 2005 and March 2006, several smaller earthquakes occurred in the Nias/Simeulue region, so the 1 year displacements in this region presumably include coseismic displacements from those small earthquakes, as well as 1 year of postseismic, aseismic motion. Stations in Aceh (in the north) show postseismic motion from the Sumatra-Andaman earthquake, stations located south of 3°N show postseismic motion from the Nias earthquake, while stations mboh and r171 are likely to be affected by postseismic motion from both earthquakes.

[17] Postseismic deformation is most evident at the SuGAr stations from northern Simeulue to the Batu islands (Figure 4b). It is largely horizontal, but significant vertical postseismic deformation also occurs close to the epicenter at LHWA and on the Batu islands at PSMK and PTLO. The amplitudes of the postseismic displacements are largest at LHWA and BSIM, the sites of largest coseismic displacements. However, the proportion of postseismic to coseismic

displacement is higher at other stations, and there are significant differences in azimuths between the postseismic and coseismic displacements (Figure 4b). Stations LHWA and BSIM were both uplifted during the Nias earthquake, but experienced postseismic subsidence for several days following the earthquake. In contrast, stations PBAI and PTLO experienced coseismic subsidence and postseismic uplift (Figure 4b). These observations of horizontal and vertical postseismic motions indicate that the afterslip had a pattern distinctly different from the coseismic slip.

### 3.4. Short-Term Preseismic Slip

[18] Near-field CGPS data from SuGAr allow us to investigate short-term preseismic and postseismic slip associated with the Nias earthquake (near-field CGPS data were not available for the Sumatra-Andaman earthquake). The SuGAr stations recorded data at 2 min intervals, rather than the typical 30 s interval, due to limited bandwidth of the available satellite communications. Because of the large geographical extent of the event and the large distances between stations we adapted kinematic GPS analysis techniques developed for open ocean marine geodetic applications [Spiess *et al.*, 1998; Chadwell and Bock, 2001], based on phase ambiguity resolution described by Blewitt [1989], and later applied to high rate GPS processing by Larson *et al.* [2003]. Tests of this approach with 1 Hz data have shown GPS antenna position repeatabilities of 10–20 mm in the horizontal [Miura *et al.*, 2002] and 20–30 mm in the vertical [Chadwell and Bock, 2001].

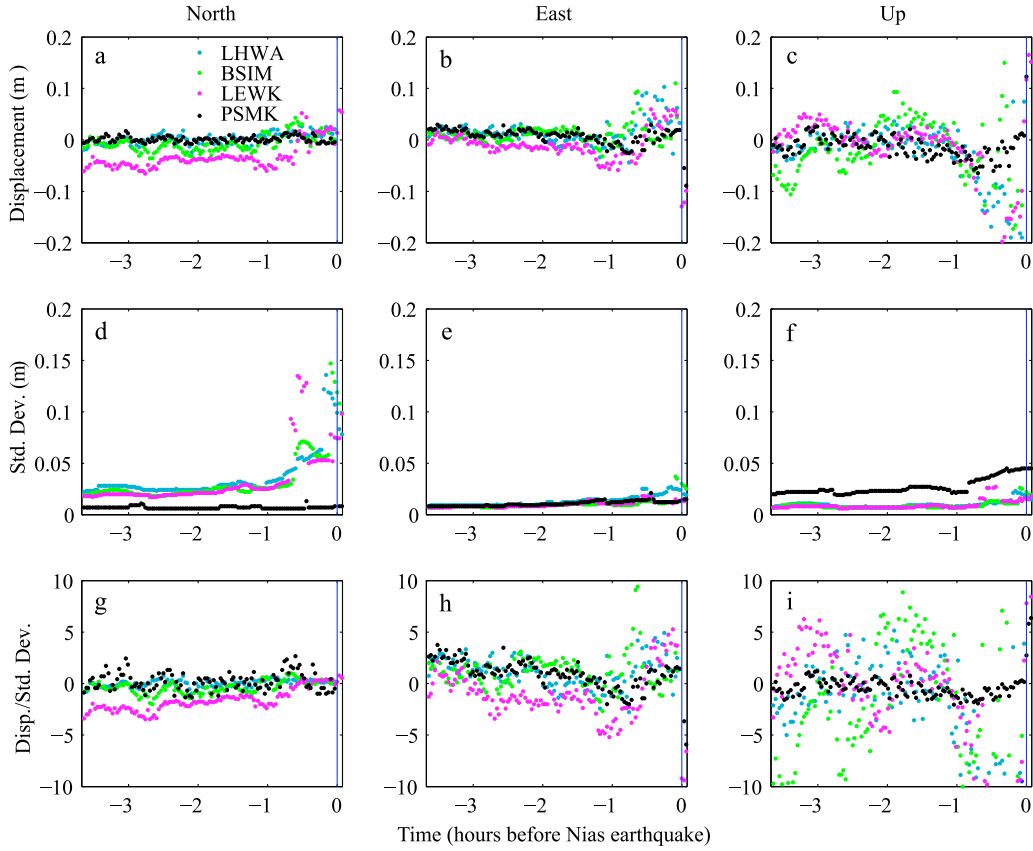


**Figure 5.** North, east, and up positions relative to (a–c) the preevent position, (d–f) the kinematic position uncertainties, and (g–i) the ratios of the preevent positions to uncertainties. Different colored dots refer to different stations, as indicated by legend. Vertical blue line at zero indicates 1609 UTC, 28 March 2005, time of Nias earthquake.

[19] We perform a kinematic network analysis of CGPS data at ten SuGAr stations (ABGS, BSIM, LEWK, LHWA, MSAI, PBAI, PSKI, PSMK, PTLO, SAMP) to estimate positions every 2 min, for 4 h before and 7 h after the Nias earthquake, using NASA Jet Propulsion Laboratory's (JPL's) GIPSY OASIS-II software [Webb and Zumberge, 1997]. Nine distant stations (located on Java, Cocos Island, Diego Garcia, Guam, India, mainland Asia, and Australia), are constrained to their ITRF2000 positions determined from combined, global solutions. The SuGAr station positions are estimated independently at each epoch by modeling them as white noise processes. The satellite orbits are from global solutions performed by JPL. Satellite clock states, receiver clock states, and L1 and L2 phase biases are estimated as white noise parameters. Tropospheric effects are modeled as random walk zenith delays. Data down to an elevation cutoff of  $2^\circ$  above the horizon are included to strengthen the satellite geometry. Solutions are performed for 26, 27, and 28 March 2005. The positions on 26 and 27 March are used to construct a sidereal signal that was removed from the positions on 28 March [Nikolaidis *et al.*, 2001; Bock *et al.*, 2004].

[20] The north, east, and up 2 min GPS positions and one-sigma uncertainties are examined for any preevent signal prior to the main seismic event. Unfortunately, the satellite constellation geometry began to degrade approximately 45 min prior to the earthquake, continued to degrade until

around the time of the earthquake, and then improved, returning to a more optimum stable geometry 30 min after the earthquake (Figure 5). Apparent position shifts prior to the main shock must therefore be interpreted with caution. We normalize the apparent shift by the position uncertainty (Figure 5d–5f) and examine the significance of any apparent north, east, and up coordinate shift. Only the apparent eastward shift at LEWK remains possibly significant (Figure 5h). Beginning at approximately 15:30 UTC the east coordinate of station LEWK increases at a nominally linear rate with a total shift of approximately 10 cm eastward by the time of the earthquake. Walker *et al.* [2005] imaged the Nias earthquake with teleseismic *P* waves and showed that the rupture propagated from the hypocenter in two different directions, first toward the north then, after a  $\sim 40$  s delay, toward the south. It is possible that the preevent displacement at LEWK, which is located at the northern end of the coseismic fault rupture, is related to this rupture pattern. In general, however, the large uncertainties around the time of the Nias earthquake make it difficult to discern a clear preseismic signal.

## 4. Modeling

### 4.1. Interseismic velocity field

[21] We model the interseismic velocity fields in Figure 2 with a modified version of the structural model from Prawirodirdjo *et al.* [1997] using the program DEFNODE

[McCaffrey, 1995], which can perform both forward modeling and inversions. We represent the structure around the subduction zone with three elastic blocks (the Sunda Shelf, the fore arc, and India/Australia) separated by the subduction fault and the Sumatra Fault. The rigid-body motion of each block is specified by a pole of rotation, and three-dimensional fault surfaces separating the blocks are specified by nodes. The slip vector  $v$  at each node is the difference between the local velocities of the blocks that are in contact across the fault. To model strain accumulation, the slip deficit (locking rate) imposed at each node is  $v\varphi$  [Savage, 1983], where the coupling coefficient  $\varphi$  is defined as the fraction of seismic slip on the fault, i.e., aseismic slip =  $v(1 - \varphi)$ . The surface deformation is calculated from the slip deficit using Okada's [1985] formulation for dislocations in an elastic half-space.

[22] During the period 1991–2001 (Figure 2a), the velocities on the southern part of the fore arc are consistent with a fully locked subduction zone ( $\varphi = 1$  from the surface down to a depth of 50 km, and  $\varphi$  decreases linearly to zero at 80 km depth). Velocities at the Batu Islands are consistent with slightly less coupling on the subduction fault. North of the Batu Islands, between 0.5°S and 3°N, the subduction fault is considerably less coupled ( $\varphi = 0.3 - 0.8$ ). It is also possible that the apparent low-locking pattern in the north was caused by an aseismic event sometime between the two occupations in 1991–1993, but to date there is no clear geodetic evidence of slow slip at the Sumatra subduction zone. Aseismic, or slow slip, events have been observed on several other subduction zones [e.g., Schwartz and Rokosky, 2007] and can take up a large percentage of the expected strain release budget at some [McCaffrey, 2008]. Natawidjaja *et al.* [2004] cautiously interpreted the alternating apparent uplift and subsidence of coral microatolls as a slow slip event on the thrust fault below the Batu Islands in 1962, but the vertical motions, specifically the rapid recovery, of that event are unlike any observed with modern GPS instruments.

[23] The velocity field in Figure 2b is derived from survey GPS data from 2001 to May 2007, and CGPS data that span approximately the same period. We fit this velocity field with an interseismic model representing a subduction fault that, south of 0.5°S, is mostly coupled from the surface down to a depth of 80 km, except for a small segment in the region of the Batu Islands (near the equator) which is allowed to slip freely in order to fit the rotated velocities there (anticlockwise rotation of the vectors indicates a decrease in the NE component which is due primarily to fault locking). The northern part of the Sumatra fore arc (north of the equator) is not modeled because the recent deformation there is dominated by the Sumatra and Nias earthquakes.

[24] Velocity vectors at the southern end of the fore arc (south of 5°S) are consistent with little or no coupling on the subduction fault. This region was the location of the  $M_w$  7.9 earthquake on 4 June 2000, a complex event that involved rupture on the subduction interface and a strike-slip fault within the downgoing oceanic slab [Abercrombie *et al.*, 2003]. Since the velocity vectors span the period 2002–2007 (2 years after the quake) and there is little strain between Enggano and the Sumatran coast, we do not think the site motions are significantly affected by postseismic afterslip from the 2000 earthquake. Instead, we suggest that this

part of the subduction zone has been slipping freely since 2002.

## 4.2. Inversion for Coseismic and Postseismic Slip

### 4.2.1. Method

[25] We use GPS-measured surface displacements to estimate slip on the fault with the Okada [1992] elastic half-space dislocation algorithm implemented in the inversion program DEFNODE [McCaffrey, 1995]. We use a structural model of the subduction zone similar to the one used by Subarya *et al.* [2006] but with additional along-strike nodes (every 0.3°–0.5° along strike) near Nias for a more refined representation of the subduction zone in that region. The top of the subducting plate is drawn near the top of the dipping seismic zone and is projected to about 80 km depth beneath the volcanic arc, with nodes at depth approximately every 5–10 km across strike. The motion of India/Australia relative to the Sunda Shelf is fixed, and slip direction on the subduction fault, along with the angular velocity of the Nias fore arc are estimated simultaneously from main shock and afterslip vectors and GPS displacement vectors. We fit coseismic slip on the fault as a Gaussian function of depth along several independent but unevenly spaced profiles across the margin (3 free parameters for each profile). Slip amplitude as a function of depth is:

$$S(z) = A \exp \left[ -(z - m_z)^2 / \sigma_z^2 \right] \quad (1)$$

where the free parameters are  $A$ , the amplitude;  $m_z$ , the depth of the mean slip; and  $\sigma_z$ , the spread in the slip. Free parameters are estimated by minimizing the quantity  $R^T C^{-1} R$ , where  $R$  is the matrix of residuals and  $C$  is the data covariance matrix. To avoid any extraneous slip not required by the data, we apply a penalty function for exceeding a prescribed seismic moment.

### 4.2.2. Slip During Nias-Simeulue Earthquake

[26] Since the GPS surveys following the Nias earthquake were performed 20–30 days after the earthquake, the measured displacements include 20–30 days of postseismic motion. We perform an inversion combining the displacements measured by survey mode GPS with displacements measured at the CGPS sites that include the coseismic displacements plus 20 days of postseismic motion. The northern boundary of the rupture zone abuts the rupture zone of the Sumatra-Andaman earthquake (Figure 6). The estimated slip distribution (Figure 6) shows that the main rupture zone, under the island of Nias, had a maximum slip of about 20 m between 10 and 30 km depth. A smaller patch of slip occurred under southeast Simeulue Island, between 15 and 40 km depths. This dual-patch nature of the rupture zone is consistent with Walker *et al.*'s [2005] imaging of the Nias earthquake with teleseismic  $P$  waves, which showed that the rupture propagated bilaterally from the hypocenter, first toward the north then, after a ~40 s delay, toward the south. Concentration of slip beneath the islands rather than beneath the ocean may have suppressed the expected tsunami [Briggs *et al.*, 2006]. Since our data includes several days of postseismic motion, our slip estimate is slightly higher than that estimated by Konca *et al.* [2007a] from a joint inversion of seismic and geodetic data. However, our additional survey GPS data provides slightly better spatial coverage, yielding more detail on the rupture patch under Nias (Figure 6),

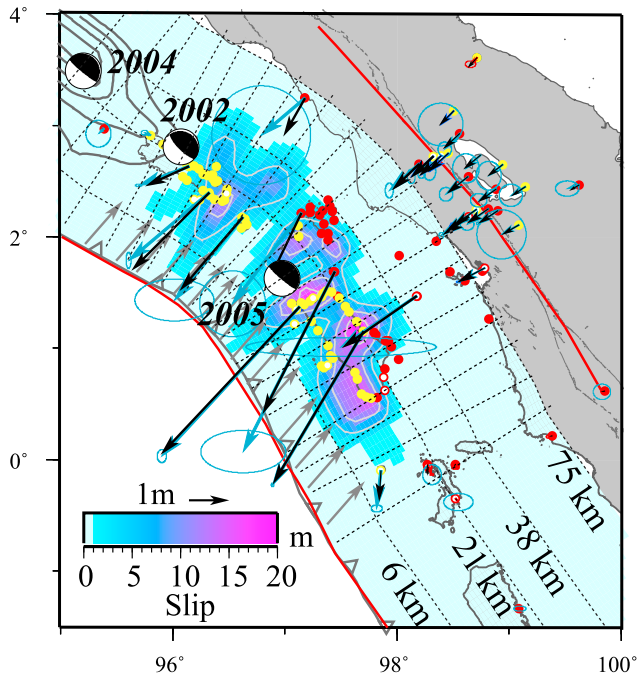


**Figure 6.** Slip distribution of Nias earthquake main shock plus 20 days of postseismic motion from inversion of displacements of continuous and survey GPS stations. Gray contour lines in the NW show the estimated rupture zone of the Sumatra-Andaman earthquake. Blue vectors show observed horizontal displacements with 95% confidence ellipses; black vectors are calculated displacements. Yellow and red dots show uplift and subsidence, respectively, and those with white centers were not fit at 2-sigma level. Gray arrows at trench show direction of coseismic slip of upper plate relative to lower, estimated in inversion. Trench-parallel dashed lines indicate slab contours, and their depths (km) are labeled at lower right. Dashed lines across the fore arc indicate model profiles used in the inversion. Same profiles are used in the inversions shown in Figures 7 and 8.

including an elongated pattern of slip that extends SE of the island. We also note that the boundary between the two main rupture patches (between south Simeulue and north Nias) is in the region of the Banyak Islands, which *Newcomb and McCann* [1987] estimated to be the northern rupture boundary of the 1861 earthquake.

[27] To the SE the rupture extends to just north of the Batu islands, coinciding with the estimated southern edge of the 1861 rupture zone [*Newcomb and McCann*, 1987]. We estimate the moment released during the main shock was  $1.2 \pm 0.03 \times 10^{22}$  N m, corresponding to a moment magnitude of  $M_w = 8.7$ . We are unable to obtain a good fit for the vector at tptn. As we mention above, tptn was not surveyed in the intervening period between the Sumatra and Nias earthquakes, and the displacement recorded there apparently includes the effect of both earthquakes.

#### 4.2.3. Postseismic Slip Following Nias-Simeulue Earthquake

[28] To examine the progression of afterslip, we perform inversions on the incremental displacements recorded at the CGPS stations during the 5 days following the March 28,

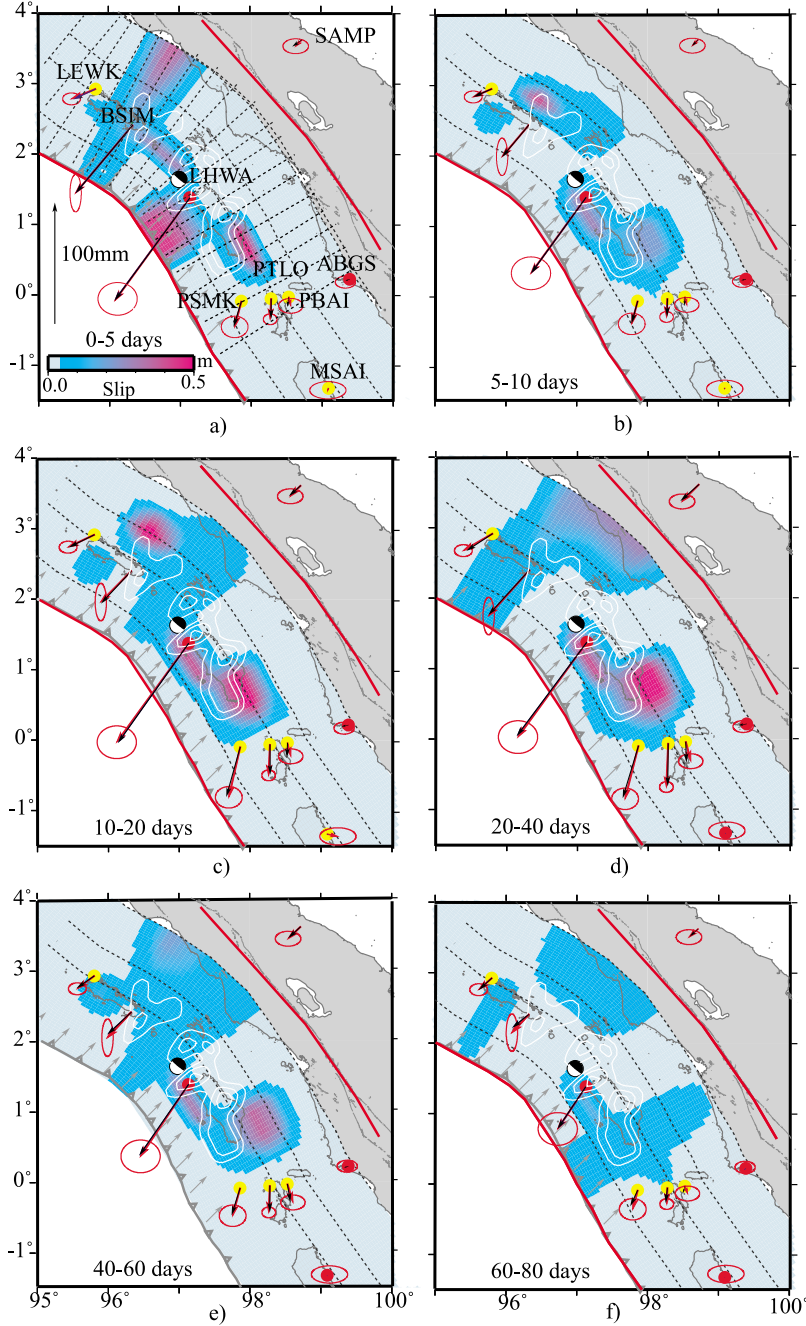
2005 Nias earthquake, for 5–10 days, 10 to 20 days, 20–40 days, 40–60 days, and 60–80 days after the earthquake. For each of these time segments we invert the incremental displacements for the afterslip distribution on the fault (Figures 7a–7f).

[29] During the first 5 days following the main shock, the largest postseismic motions are observed on northern Nias and Southern Simeulue (Figure 7a). Significant postseismic motion is also observed outside of the main rupture zone at SAMP, and at the Batu Islands (PSMK, PTLO, and PBAI). Inversion of these 5 days of postseismic motion shows that afterslip migrated updip from Nias and downdip from Simeulue, as well as laterally SE of the main rupture area. Maximum estimated slip during this period reached 0.45 m, occurring just updip of Nias (Figure 7a). Between 5 and 10 days after the main shock, two distinct patches of afterslip developed, concentrated downdip from Simeulue, on the deeper part of the fault (below 40 km), and SE of Nias (Figures 7b), with the estimated slip reaching a maximum of 0.4 m.

[30] Over the next 50 days (10–60 days after the main shock), the northern patch migrates downdip, constrained by continued motion at SAMP, while the southern patch, constrained by postseismic motion at PSMK, PTLO, and PBAI, is concentrated just NW of the Batu islands (Figures 7c and 7d). Between 10 and 20 days, the maximum estimated slip on the fault is 0.5 m. Between 20 and 80 days after the main shock, we estimate the maximum slip to be about 0.5 m every 20 days (Figures 7d–7f). After 60 days, the patches of afterslip begin to decrease in size (Figure 7f). Between 80 and 100 days after the earthquake, we estimate less than 0.2 m, and between 100 and 120 days, less than 0.1 m of afterslip on the fault (not shown).

[31] We also perform inversions to estimate afterslip using the postseismic displacements measured at the survey and continuous GPS stations during the first year (2005–2006) and second year (2006–2007) following the Nias earthquake (Figure 8). Our analysis of the CGPS data shows that most of the postseismic motion occurred in the first 100 days after the earthquake, so the slip distribution in Figure 8a can be seen as an approximate sum of the postseismic slip shown in Figures 7a–7f. We note that the GPS surveys following the Nias earthquake were begun a few days after the main shock. To be consistent, the CGPS data included in these versions were taken for the same time interval covered by the survey GPS stations, therefore afterslip occurring during the first few days directly following the earthquake (i.e., as seen in Figure 7a) are not seen in Figure 8a.

[32] In the Aceh region, we measure displacements of 0.3–0.5 m for the year following the Sumatra-Andaman earthquake main shock (Figure 8a), corresponding to afterslip of up to 8 m on the subduction fault, concentrated updip from the main rupture zone (Figure 8a). Unfortunately, we do not have data from the Andaman and Nicobar islands to study afterslip further north. The slip distribution in Figure 8a shows a patch of afterslip north of Simeulue, constrained by the GPS vectors at stations mb0h and r171, which are presumably affected by postseismic motion from the Sumatra-Andaman earthquake. During the 1 year period following the Nias earthquake, several  $M_w \geq 6$  earthquakes occurred in the area, including a cluster of events located between Nias and Simeulue (Figure 8a). Some of the apparent afterslip in this region shown by our model is likely

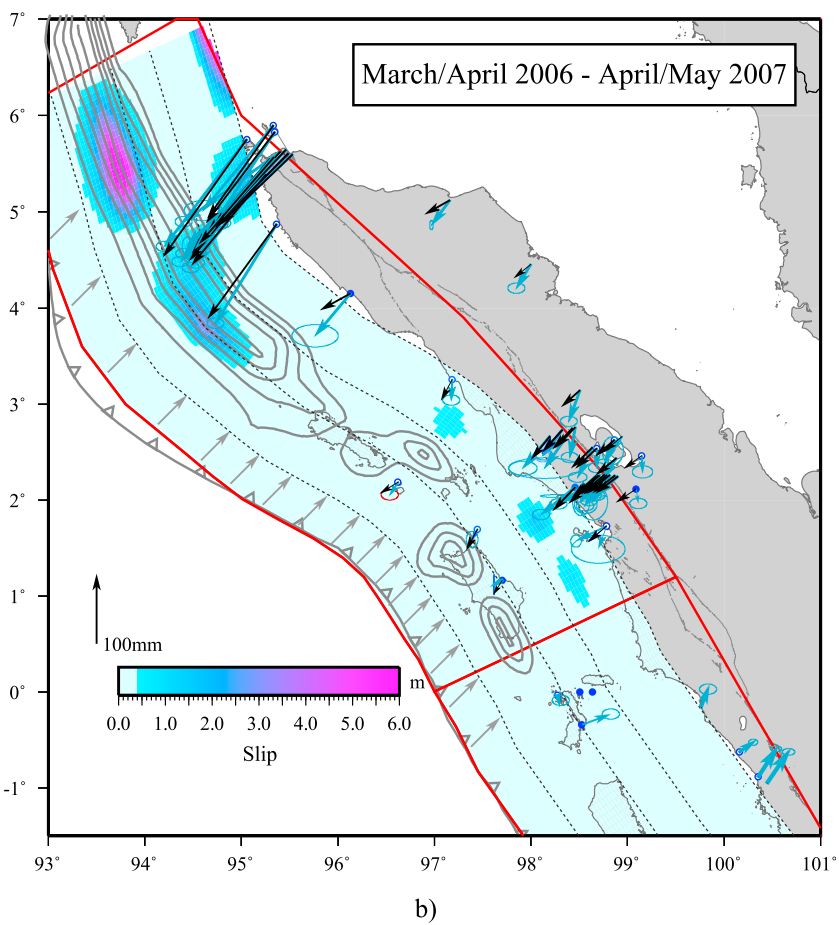
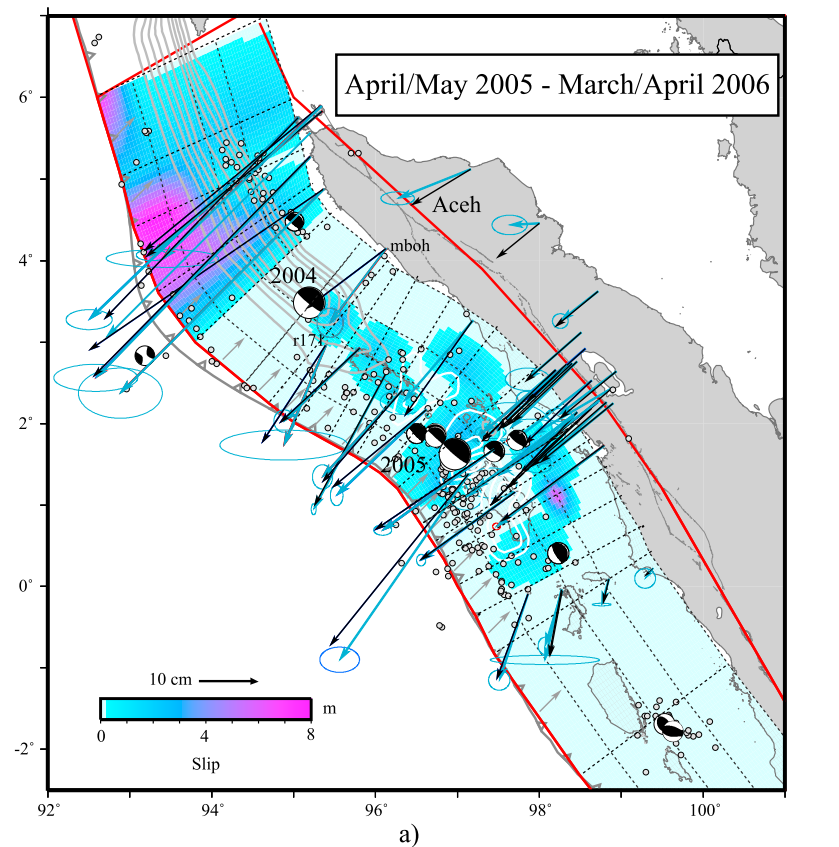


**Figure 7.** Postseismic progression of Nias earthquake afterslip at (a) 0–5 days, (b) 5–10 days, (c) 10–20 days, (d) 20–40 days, (e) 40–60 days, (f) 60–80 days, and (g) 80–100 days after the main shock. Light contour lines show Nias earthquake coseismic slip distribution calculated in Figure 6. Red vectors show observed horizontal displacements with 95% confidence ellipses; black vectors are calculated displacements. Red and yellow dots show vertical data.

to be due to these earthquakes. *Briggs et al.* [2006] noted that this area just north of Nias also separates the two principal rupture patches of the Nias earthquake and coincides with a discontinuity in bathymetry of the outer arc ridge, and a misalignment of the Nias earthquake vertical coseismic deformation contours, suggesting a possible tear in the subducting slab. Elsewhere on the rupture zone, our modeling shows that afterslip from the Nias earthquake is concentrated downdip from the main rupture. Compared to

the 9 month afterslip estimated by *Hsu et al.* [2006], our estimate shows more afterslip occurring downdip instead of updip of the seismic rupture zone, a result of the added constraint of observations from survey stations on Sumatra.

[33] Preliminary analysis of displacements spanning the period April 2006 to May 2007 computed from survey data showed that displacement rates north of the equator were still significantly different from their preearthquake interseismic velocities, so we attempt to model the deformation

**Figure 8**

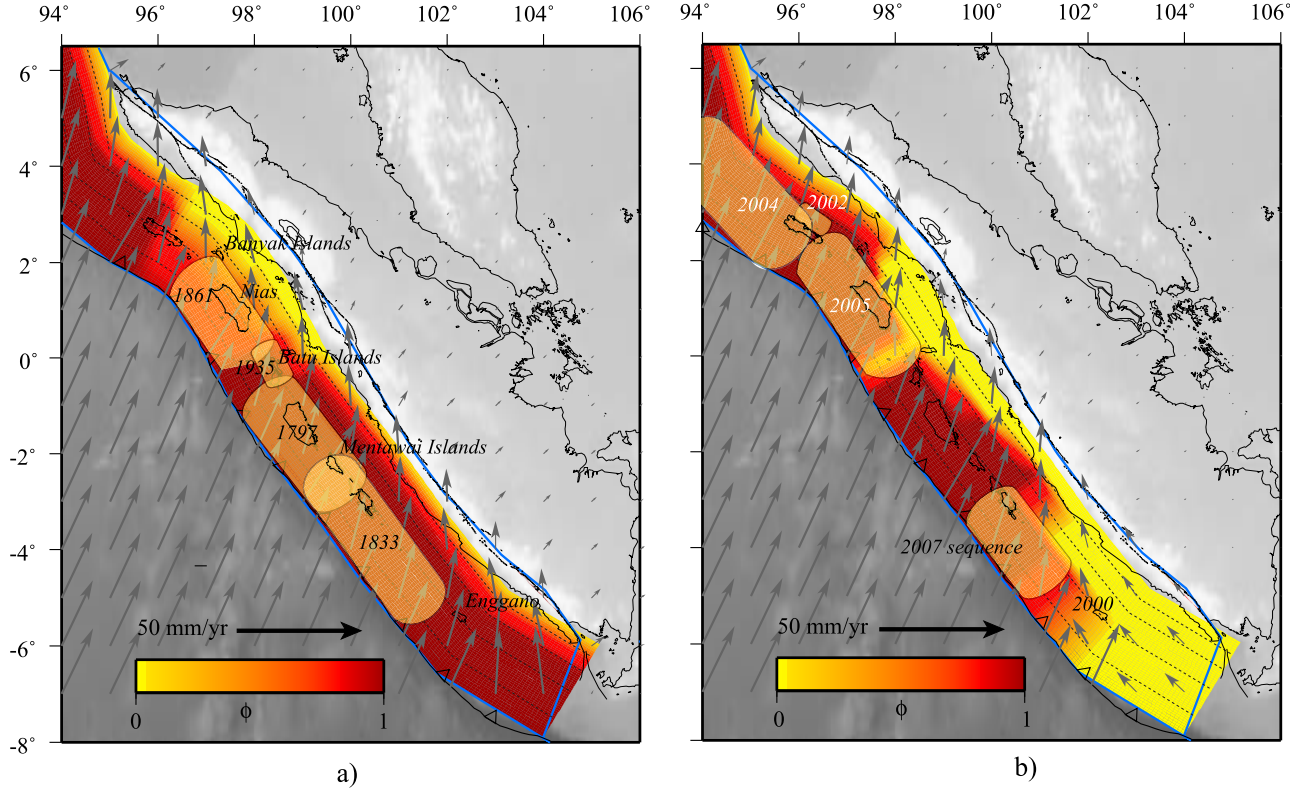


**Figure 9.** (a) Modeled interseismic velocity field (gray arrows) for period leading up to 21st century. Shading on the fore arc represents the value of the coupling coefficient  $\varphi$  used in model. Yellow patches show estimated rupture zones of significant subduction earthquakes. (b) Modeled current velocity field (gray arrows). Shading on the fore arc represents coupling coefficient values. Yellow patches show rupture zones of recent subduction earthquakes.

as a continuation of afterslip. Our best fitting model for these displacements are shown in Figure 8b. In the Nias region, the remaining afterslip is downdip of the Nias earthquake rupture zone. Stations on the northern tip of Aceh are still experiencing large postseismic motions (on the order of 0.1 m during the second year after the Sumatra-Andaman earthquake), consistent with afterslip of several meters on the subduction zone.

## 5. Discussion

[34] More than 15 years of GPS data from the Sumatra subduction zone, originating with surveys performed in the early 1990s and supplemented by continuous GPS data, in situ coral uplift data, and remote sensing, provide increasingly detailed information on the subduction zone behavior. These observations have spanned the end of one interseismic earthquake cycle and the beginning of a new one as well as two great earthquakes and the accompanying post-

seismic motion, allowing us to construct a representation of the deformation during the past earthquake cycle.

[35] In Figure 9 we summarize and past and current scenarios for the Sumatra subduction zone based on our results. Figure 9a shows the predicted surface horizontal velocity field pre-2001, during the interseismic phase. We assume that this velocity field approximates the average, long-term interseismic deformation in the region. The  $\varphi$  distribution in Figure 9a is reproduced from Figure 2a. Most of the subduction interface is locked but there are some patches that have low coupling. For example, in Figure 9a we modeled the subduction zone between 1°S and 2°N to have a low coupling coefficient ( $\varphi$ ) to fit GPS survey data from 1991 to 2001 (see also Figure 2a). It is unclear whether a low coupling coefficient is a permanent characteristic of this segment of the subduction zone, but the segment coincides with the rupture zone of the 1861 earthquake, suggesting that the segmentation is real and may be controlled by lasting properties of the fault interface.

**Figure 8.** (a) Afterslip distribution estimated from the 1 year accumulated displacement following Nias EARTHQUAKE (2005–2006). (b) Afterslip distribution estimated from the displacements accumulated during the second year following Nias earthquake (2006–2007). Blue vectors show observed horizontal displacements with 95% confidence ellipses; black vectors are calculated displacements. Gray contour lines show Sumatra-Andaman earthquake slip distribution; white contour lines show Nias earthquake slip distribution. Yellow lines delineate the fore-arc block. Gray dots show epicenters of earthquakes in the region that occurred in the 1 year period following the Nias earthquake; focal mechanisms are given for  $M_w > 6$  earthquakes. Large focal mechanisms are the 2004 Sumatra and 2005 Nias earthquakes.

[36] Figure 9b shows the current velocity field south of the equator (with  $\varphi$  distribution reproduced from Figure 2b). North of the equator in Figure 9b we show a possible scenario for the velocity field and  $\varphi$  distribution once the postseismic motions subside. Current velocities at the Batu Islands are consistent with little or no coupling on the fault interface at that location. At the southern end of the subduction zone, the velocity at Enggano is currently also consistent with little or no coupling on the subduction zone. Chlieh *et al.* [2008] also note the low coupling regions of the Batu Islands and Enggano. However, their interseismic model differs from ours in their inclusion of a low coupling region updip of the locked regions. In Savage's [1983, 1996] description of an elastic dislocation model for strain accumulation for a subduction zone, he noted that the model was intended to approximate the deformation caused by aseismic slip on the subduction fault downdip from the locked patch. McCaffrey [2002] showed that implementing a free-slip updip of the locked region in an elastic dislocation model results in improbable strain rates in the updip part of the overriding wedge. A detailed discussion is given by McCaffrey [2002].

[37] Our analysis of survey GPS data from the 1990s suggests that low coupling at the Batu Islands and Enggano is a relatively recent feature of the subduction zone. It appears that, while the spatial segmentation of the subduction zone is preserved, the degree of coupling on the subduction zone may vary with time. The mechanism for this change is unclear, but the change may be triggered by seismic rupture of the subduction fault.

[38] The main rupture of the Nias earthquake was under the island of Nias, with a smaller patch of slip under southeastern Simeulue Island. Concentration of slip beneath the islands rather than beneath the ocean may have suppressed the expected tsunami [Briggs *et al.*, 2006]. Konca *et al.* [2007a] estimated the coseismic slip of the Nias earthquake using a combination of CGPS data from the SuGAR array and vertical displacement measurements from coral reefs above the fault rupture. In contrast, our estimation of slip from the Nias earthquake includes data from survey mode GPS. Our data therefore do not have the temporal resolution of Konca *et al.*'s [2007a], but we have better spatial coverage. Correspondingly, our estimate of fault slip during the earthquake is slightly higher than theirs because ours includes several days of postseismic motion. Our slip estimate yields more detail for the rupture patch under Nias (Figure 6), and includes an elongated pattern of slip that extends SE of the island.

[39] The 2005 (Nias) rupture zone was similar to the (estimated) rupture zone of the 1861 earthquake, which produced a large tsunami. The narrow boundary between it and the 2004 rupture zone is located near northern Simeulue. This is also the location of an  $M_w$  7.3 earthquake in 2002, and a change in the trench strike; the trench rotation is echoed in the strike of Simeulue Island as well as in the strike of the 2002 rupture plane. DeShon *et al.* [2005], without supporting evidence, suggest that this region marks the southern edge of the Andaman microplate and as such, acts as a long-lived, natural barrier to seismic rupture. An abrupt change in the azimuths of slip vectors of under-thrusting earthquakes suggests instead that the structural boundary of the southern edge of the Andaman block is at 6N [see Subarya *et al.*, 2006, Electronic Supplement 2].

Moreover, it should be remembered that the northwestern boundary of slip in the 1861 event is only approximate. For some reason, possibly circular, many researchers draw the northwestern edge of rupture of the 1861 event through Simeulue Island, even though Newcomb and McCann [1987], based on maximum intensities, estimated the rupture to fall between the "Banyak and Pini Islands". The Banyak Islands are more than 100 km southeast of central Simeulue. While the tsunami reached Simeulue in 1861, observed high tsunami runups occurred along the Sumatra coast > 250 km southeast of the southernmost slip in the 2004 Aceh earthquake [Choi *et al.*, 2006] and are not precise indicators of fault slip.

[40] Our analysis of 2 min kinematic station positions for the 4 h immediately before the Nias earthquake shows possible eastward shift at station LEWK starting approximately 30 min before the main shock. This observation of one component at one station is not decisive, however, and we must conclude that the large uncertainties preclude a clear observation of preseismic motions.

[41] Our observations show that the Sumatra and Nias earthquakes were followed by several months of postseismic motion. The postseismic motion takes place as afterslip on parts of the fault that did not slip seismically, most of it taking place during the first few weeks after the main shock, and decaying logarithmically, consistent with rate-strengthening friction law, as described by Marone [1998]. Modeling of postseismic displacements from Aceh region suggests that postseismic motion from the Sumatra-Andaman earthquake is largely concentrated on the shallow part of the subduction fault, updip from the main rupture zone. The postseismic motion from the Nias earthquake is consistent with aseismic slip on the fault at the rate of 100 mm/d for the first 10 days, slowing down to about 25 mm/d for the next few months. Afterslip following the Nias earthquake on the subduction fault migrated significantly from the region of coseismic slip, with much of it concentrated downdip from the main rupture zone, and some migrating laterally SE toward the Batu Islands. The post-seismic afterslip occurs on parts of the subduction fault that were locked but did not slip during the main shocks.

[42] Our observations confirm that the Sumatra megathrust is highly segmented, as noted by previous studies [e.g., Prawirodirdjo *et al.*, 1997; Sieh and Natawidjaja, 2000, Chlieh *et al.*, 2008]. The segmentation is apparent in the interseismic velocity field as well as the seismic rupture zones, and is probably long-lasting. More work is still needed in order to understand the mechanisms that cause segmentation, but recent studies suggest that the segmentation is related to geometry/characteristics that continue at depth [Abercrombie *et al.*, 2003; DeShon *et al.*, 2005; Briggs *et al.*, 2006] and may thus have more to do with structural anomalies (e.g., tears in the slab, subducted fossil fracture zones) than with properties of the subduction interface (e.g., fluid pore pressures, temperature).

## 6. Summary

[43] We summarize the different domains of the Sumatra subduction zone observed in our study, north to south, as follows.

[44] 1. The northernmost section, comprising the Sumatra-Andaman segment ( $2^{\circ}\text{N}$ – $10^{\circ}\text{N}$ ), ruptured during the catastrophic 2004 earthquake.

[45] 2. The rupture zones of the Sumatra-Andaman and Nias-Simeulue earthquakes are separated by a narrow zone near northern Simeulue, where earthquakes occurred in 1976 ( $M_w$  7.0) and 2002 ( $M_w$  7.3).

[46] 3. The Nias-Simeulue segment ( $0^{\circ}$ – $2^{\circ}\text{N}$ ), abutting the Sumatra-Andaman segment to the southeast, ruptured in 1861 and 2005 (the Nias earthquake). The Nias-Simeulue earthquake ruptured as two distinct patches, located northwest and southeast of the Banyak islands. After the Nias earthquake, several  $M_w > 6$  earthquakes occurred in the region of the Banyak Islands, between Nias and Simeulue. This may be the site of a tear in the subducting slab [Briggs et al., 2006] which acts as a natural barrier to rupture.

[47] 4. The Batu Islands region ( $0.5^{\circ}\text{S}$ ) was the site of an  $M$  7.7 (estimated) earthquake in 1935 and an aseismic slip event in 1962 [Natawidjaja et al., 2004]. The velocity field in the 1990s here was consistent with partial to full coupling on the subduction zone underneath, but the current velocity vectors on the Batu Islands indicate little or no coupling. We speculate that this patch is also a barrier to rupture.

[48] 5. The Mentawai segment ( $0.5^{\circ}\text{S}$  to  $5^{\circ}\text{S}$ ) ruptured in 1797 and 1833. The 1833 earthquake was estimated to have been about  $M_w$  8.8 [Newcomb and McCann, 1987] and was reportedly accompanied by 3–4 m high tsunamis. In September 2007 this segment experienced a sequence of large earthquakes [Sladen et al., 2007; Meltzner et al., 2007; Natawidjaja et al., 2007; Konca et al., 2007b]. Up to that time, the deformation pattern on the Mentawai islands is consistent with a fully locked subduction interface, and Natawidjaja et al. [2006] noted that coral heads in the region indicate that interseismic strains accumulated along this segment of the subduction zone have probably approached or exceeded levels relieved in 1797 and 1833.

[49] 6. The southernmost segment of the Sumatra subduction zone, the Enggano segment ( $5^{\circ}\text{S}$  to  $6.5^{\circ}\text{S}$ ), ruptured in an  $M_w$  7.9 earthquake in June 2000. This earthquake occurred at the edge of the rupture area of the 1833 earthquake and was a complex event that broke part of the subduction interface, rupturing to the southeast away from the 1833 earthquake, but also involved rupture on a deep, vertical strike-slip fault [Abercrombie et al., 2003]. This segment, like the Batu Islands region, has a different interseismic deformation pattern now than it did in the 1990s (Figure 2). The interseismic deformation pattern in the 1990s was consistent with a locked subduction zone, whereas the current deformation is more consistent with a freely slipping subduction interface. The subduction zone in the Enggano region may be similar to that underneath the Batu islands.

[50] **Acknowledgments.** We thank Kerry Sieh, John Galetzka, and Danny Natawidjaja, and their colleagues at the Caltech Tectonics Observatory and LIPI, who established and are maintaining the Sumatra GPS Array, and the BAKOSURTANAL surveyors who performed the GPS field work in Indonesia. McCaffrey's participation was supported by RPI. SCEC/SCIGN (John McRaney) and NSF Geophysics (Robin Reichlin) expedited emergency funding in response to the great Sumatra-Andaman event, which covered most of the costs of the three field GPS surveys described in this paper. This study was also supported by NASA grant NNX08AF70G.

## References

- Abercrombie, R. E., M. Antolik, and G. Ekstrom (2003), The 2000 June 2000  $M_w$  7.9 earthquakes south of Sumatra: Deformation in the India-Australia plate, *J. Geophys. Res.*, 108(B1), 2018, doi:10.1029/2001JB000674.
- Altamimi, Z., X. Collilieux, J. Legrand, B. Garayt, and C. Boucher (2007), ITRF2005: A new release of the International Terrestrial Reference Frame based on time series of station positions and Earth orientation parameters, *J. Geophys. Res.*, 112, B09401, doi:10.1029/2007JB004949.
- Ammon, C. J., et al. (2005), Rupture process of the 2004 Sumatra-Andaman earthquake, *Science*, 308, 1133–1139, doi:10.1126/science.1112260.
- Banerjee, P., F. F. Pollitz, and R. Bürgmann (2005), The size and duration of the Sumatra-Andaman earthquake from far-field static offsets, *Science*, 308, 1769–1772, doi:10.1126/science.1113746.
- Blewitt, G. (1989), Carrier phase ambiguity resolution for the Global Positioning System applied to geodetic baselines up to 2000 km, *J. Geophys. Res.*, 94, 10,187–10,203, doi:10.1029/JB094B08p10187.
- Bock, Y., L. Prawirodirdjo, J. F. Genrich, C. W. Stevens, R. McCaffrey, C. Subarya, S. S. O. Puntodewo, and E. Calais (2003), Crustal motion in Indonesia from Global Positioning System measurements, *J. Geophys. Res.*, 108(B8), 2367, doi:10.1029/2001JB000324.
- Bock, Y., L. Prawirodirdjo, and T. I. Melbourne (2004), Detection of arbitrarily large dynamic ground motions with a dense high-rate GPS network, *Geophys. Res. Lett.*, 31, L06604, doi:10.1029/2003GL019150.
- Boehm, J., A. Niell, P. Tregoning, and H. Schuh (2006), Global Mapping Function (GMF): A new empirical mapping function based on numerical weather model data, *Geophys. Res. Lett.*, 33, L07304, doi:10.1029/2005GL025546.
- Briggs, R., et al. (2006), Deformation and slip along the Sunda megathrust in the great 2005 Nias-Simeulue earthquake, *Science*, 311, 1897–1901, doi:10.1126/science.1122602.
- Chadwell, C. D., and Y. Bock (2001), Direct estimation of absolute precipitable water in oceanic regions by GPS tracking of a coastal buoy, *Geophys. Res. Lett.*, 28, 3701–3704, doi:10.1029/2001GL013280.
- Chlieh, M., et al. (2007), Coseismic slip and afterslip of the great  $M_w$  9.15 Sumatra-Andaman earthquake of 2004, *Bull. Seismol. Soc. Am.*, 97(1A), S152–S173, doi:10.1785/0120050631.
- Chlieh, M., J. P. Avouac, K. Sieh, D. H. Natawidjaja, and J. Galetzka (2008), Heterogeneous coupling of the Sumatran megathrust constrained by geodetic and paleogeodetic measurements, *J. Geophys. Res.*, 113, B05305, doi:10.1029/2007JB004981.
- Choi, B. H., S. J. Hong, and E. Pelinovsky (2006), Distribution of runup heights of the December 26, 2004 tsunami in the Indian Ocean, *Geophys. Res. Lett.*, 33, L13601, doi:10.1029/2006GL025867.
- DeShon, H. R., E. R. Engdahl, C. H. Thurber, and M. Brudzinski (2005), Constraining the boundary between the Sunda and Andaman subduction systems: Evidence from the 2002  $M_w$  7.3 northern Sumatra earthquakes and aftershock relocations of the 2004 and 2005 great earthquakes, *Geophys. Res. Lett.*, 32, L24307, doi:10.1029/2005GL024188.
- Fitch, T. J. (1972), Plate convergence, transcurrent faults and internal deformation adjacent to Southeast Asia and the western Pacific, *J. Geophys. Res.*, 77, 4432–4460, doi:10.1029/JB077i023p04432.
- Gahalaut, V. K., B. Nagarajan, J. K. Catherine, and S. Kumar (2006), Constraints on 2004 Sumatra-Andaman earthquake rupture from GPS measurements in Andaman-Nicobar Islands, *Earth Planet. Sci. Lett.*, 242, 365–374, doi:10.1016/j.epsl.2005.11.051.
- Genrich, J. F., Y. Bock, R. McCaffrey, L. Prawirodirdjo, C. W. Stevens, S. S. O. Puntodewo, C. Subarya, and S. Wdowinski (2000), Slip distribution at the northern Sumatra Fault System, *J. Geophys. Res.*, 105, 28,327–28,341, doi:10.1029/2000JB900158.
- Hsu, Y.-J., M. Simons, J.-P. Avouac, J. Galetzka, K. Sieh, M. Chlieh, D. Natawidjaja, L. Prawirodirdjo, and Y. Bock (2006), Frictional afterslip following the 2005 Nias-Simeulue earthquake, Sumatra, *Science*, 312, 1921–1926, doi:10.1126/science.1126960.
- Jade, S., M. B. Ananda, P. D. Kumar, and S. Banerjee (2005), Co-seismic and post-seismic displacements in Andaman and Nicobar Islands from GPS measurements, *Curr. Sci.*, 88, 1980–1984.
- Konca, A. O., V. Hjorleifsdottir, T. Song, J.-P. Avouac, D. V. Helmberger, C. Ji, K. Sieh, R. Briggs, and A. Meltzner (2007a), Rupture kinematics of the 2005  $Mw$  8.6 Nias-Simeulue earthquake from the joint inversion of seismic and geodetic data, *Bull. Seismol. Soc. Am.*, 97, S307–S322, doi:10.1785/0120050632.
- Konca, A. O., et al. (2007b), Rupture kinematics of Mw 8.4 South Pagai earthquake, Sumatra, from joint inversion of seismic and geodetic data, *Eos Trans. AGU*, 88(52), Fall Meet. Suppl., Abstract U53A-07.
- Konca, A. O., et al. (2008), Partial rupture of a locked patch of the Sumatra megathrust during the 2007 earthquake sequence, *Nature*, 456, 631–635, doi:10.1038/nature07572.

- Larson, K., P. Bodin, and J. Gomberg (2003), Using 1 Hz GPS data to measure deformations caused by the Denali Fault earthquake, *Science*, **300**, 1421–1424, doi:10.1126/science.1084531.
- Marone, C. (1998), Laboratory-derived friction laws and their application to seismic faulting, *Annu. Rev. Earth Planet. Sci.*, **26**, 643–696, doi:10.1146/annurev.earth.26.1.643.
- McCaffrey, R. (1992), Oblique plate convergence, slip vectors, and forearc deformation, *J. Geophys. Res.*, **97**, 8905–8915, doi:10.1029/92JB00483.
- McCaffrey, R. (1995), DEFNODE users guide, Rensselaer Polytech. Inst., Troy, New York. (Available at <http://www.rpi.edu/~mccaffr/defnode/>)
- McCaffrey, R. (2002), Crustal block rotations and plate coupling, in *Plate Boundary Zones*, *Geodyn. Ser.*, vol. 30, edited by S. Stein and J. Freymueller, pp. 101–122, doi:10.1029/030GD06, AGU, Washington, D. C.
- McCaffrey, R. (2008), The impact of slow-slip events on seismic moment release in subduction zones, *Eos Trans. AGU*, **89**(23), Jt. Assem. Suppl. Abstract G33B-08.
- Meltzner, A. J., K. Sieh, M. Abrams, D. C. Agnew, K. W. Hudnut, J.-P. Avouac, and D. Natawidjaja (2006), Uplift and subsidence associated with the great Aceh-Andaman earthquake of 2004, *J. Geophys. Res.*, **111**, B02407, doi:10.1029/2005JB003891.
- Meltzner, A. J., K. Sieh, D. H. Natawidjaja, A. O. Konca, and A. Sladen (2007), Uplift and subsidence during the September 2007 Mentawai earthquakes from field observations, *Eos Trans. AGU*, **88**(52), Fall Meet. Suppl., Abstract U54A-02.
- Miura, S., T. Sato, K. Tachibana, Y. Satake, and A. Hasegawa (2002), Strain accumulation in and around Ou Backbone Range, northeastern Japan as observed by a dense GPS network, *Earth Planets Space*, **54**, 1071–1076.
- Natawidjaja, D. H., K. Sieh, S. N. Ward, H. Cheng, R. L. Edwards, J. Galetzka, and B. W. Suwargadi (2004), Paleogeodetic records of seismic and aseismic subduction from central Sumatran microatolls, Indonesia, *J. Geophys. Res.*, **109**, B04306, doi:10.1029/2003JB002398.
- Natawidjaja, D. H., K. Sieh, M. Chlieh, J. Galetzka, B. W. Suwargadi, H. Cheng, R. L. Edwards, J.-P. Avouac, and S. N. Ward (2006), Source parameters of the great Sumatran megathrust earthquakes of 1797 and 1833 inferred from coral microatolls, *J. Geophys. Res.*, **111**, B06403, doi:10.1029/2005JB004025.
- Natawidjaja, D., K. Sieh, J. Galetzka, B. W. Suwargadi, R. L. Edwards, H. Cheng, C. Shen, and C. Mohamed (2007), A 700-year-long paleoseismic context for the Sumatran megathrust earthquakes of 2007, *Eos Trans. AGU*, **88**(52), Fall Meet. Suppl., Abstract U53A-01.
- Newcomb, K. R., and W. R. McCann (1987), Seismic history and seismotectonics of the Sunda Arc, *J. Geophys. Res.*, **92**, 421–439, doi:10.1029/JB092iB01p00421.
- Nikolaidis, R. (2002), Observation of geodetic and seismic deformation with the Global Positioning System. Ph.D. thesis, Univ. of Calif., San Diego.
- Nikolaidis, R., Y. Bock, P. Shearer, P. J. de Jonge, D. C. Agnew, and M. Van Domselaar (2001), Seismic wave observations with the Global Positioning System, *J. Geophys. Res.*, **106**, 21,897–21,916, doi:10.1029/2001JB000329.
- Okada, Y. (1985), Surface deformation due to shear and tensile faults in a half-space, *Bull. Seismol. Soc. Am.*, **75**, 1135–1154.
- Okada, Y. (1992), Internal deformation due to shear and tensile faults in a half-space, *Bull. Seismol. Soc. Am.*, **82**, 1018–1040.
- Prawirodirdjo, L., et al. (1997), Geodetic observations of interseismic strain segmentation at the Sumatra subduction zone, *Geophys. Res. Lett.*, **24**, 2601–2604, doi:10.1029/97GL52691.
- Savage, J. C. (1983), A dislocation model of strain accumulation and release at a subduction zone, *J. Geophys. Res.*, **88**, 4984–4996, doi:10.1029/JB088iB06p04984.
- Savage, J. C. (1996), Comment on “The stress state implied by dislocation models of subduction deformation” by J. J. Douglass and B. A. Buffet, *Geophys. Res. Lett.*, **23**, 2709–2710, doi:10.1029/96GL02374.
- Scherneck, H.-G., J. M. Johansson, and F. H. Webb (2000), *Ocean loading tides in GPS and rapid variations of the frame origin, in Geodesy Beyond 2000: The Challenges of the First Decade: IAG General Assembly, Birmingham, July 19–30, 1999, Int. Assoc. Geod. Symp.*, vol. 121, edited by K.-P. Schwarz, pp. 32–40, Springer, Berlin.
- Schmid, R., P. Steigenberger, G. Gendt, M. Ge, and M. Rothacher (2007), Generation of a consistent absolute phase center correction model for GPS receiver and satellite antennas, *J. Geod.*, **81**(12) 781–798, doi:10.1007/s00190-007-0148-y.
- Schwartz, S. Y., and J. M. Rokosky (2007), Slow slip events and seismic tremor at circum-Pacific subduction zones, *Rev. Geophys.*, **45**, RG3004, doi:10.1029/2006RG000208.
- Sieh, K., and D. Natawidjaja (2000), Neotectonics of the Sumatran fault, Indonesia, *J. Geophys. Res.*, **105**, 28,295–28,326, doi:10.1029/2000JB900120.
- Sieh, K., et al. (2008), Earthquake supercycles inferred from sea-level changes recorded in the corals of West Sumatra, *Science*, **322**, 1674–1678, doi:10.1126/science.1163589.
- Sladen, A., et al. (2007), The 12 September 2007,  $M_w = 7.9$  Pagai-Sipora earthquake, an impulsive rupture on the central Sumatra megathrust, *Eos Trans. AGU*, **88**(52), Fall Meet. Suppl., Abstract U51A-05.
- Socquet, A., C. Vigny, N. Chamot-Rooke, W. Simons, C. Rangin, and B. Ambrosius (2006), India and Sunda plates motion and deformation along their boundary in Myanmar determined by GPS, *J. Geophys. Res.*, **111**, B05406, doi:10.1029/2005JB003877.
- Spiess, F. N., C. D. Chadwell, J. A. Hildebrand, L. E. Young, G. H. Purcell, and H. Drager (1998), Precise GPS/acoustic positioning of seafloor reference points for tectonic studies, *Phys. Earth Planet. Inter.*, **108**, 101–112, doi:10.1016/S0031-9201(98)00089-2.
- Stein, S., and E. A. Okal (2005), Speed and size of the Sumatra earthquake, *Nature*, **434**, 581–582, doi:10.1038/434581a.
- Subarya, C., M. Chlieh, L. Prawirodirdjo, J.-P. Avouac, Y. Bock, K. Sieh, A. J. Meltzner, D. H. Natawidjaja, and R. McCaffrey (2006), Plate-boundary deformation associated with the great Aceh-Andaman earthquake, *Nature*, **440**, 46–51, doi:10.1038/nature04522.
- Walker, K. T., M. Ishii, and P. M. Shearer (2005), Rupture details of the 28 March 2005 Sumatra  $M_w = 8.6$  earthquake imaged with teleseismic  $P$  waves, *Geophys. Res. Lett.*, **32**, L24303, doi:10.1029/2005GL024395.
- Webb, F., and J. Zumberge (1997), An introduction to GPSY/OASIS-II, *JPL Publ.*, D-1108.
- 
- Y. Bock and L. Prawirodirdjo, Cecil H. and Ida M. Green Institute of Geophysics and Planetary Physics, Scripps Institution of Oceanography, La Jolla, CA 92093, USA. (linette@gpsmail.ucsd.edu)
- C. D. Chadwell, Marine Physical Laboratory, Scripps Institution of Oceanography, La Jolla, CA 92093, USA.
- R. McCaffrey, Department of Earth and Environmental Sciences, Rensselaer Polytechnic Institute, Troy, NY 12180, USA.
- C. Subarya, National Coordinating Agency for Surveys and Mapping, JL Raya Jakarta-Bogor KM46, Cibinong, 16911 Indonesia.